Formation Control of Autonomous Air Vehicles

Valter Roldão

Abstract—**This paper presents a strategy for motion coordination of a group of autonomous vehicles using a leader-following approach. The coordination is separated in two steps: a first step in which the motion of the leader is passed to a trajectory planner and a second step in which the trajectories generated are passed to the vehicles.**

Using a Lyapunov-based approach, the planner prescribes the motion of a group of virtual vehicles, modelled as unicycles, so as to keep the leader in a predefined configuration in their reference frame. By constraining the motion of these vehicles, the planner naturally guarantees the generation of adequate formation trajectories, bypassing the onerous task of obtaining path parametrizations.

In the second step the trajectories of the virtual vehicles are used as reference trajectories for a group of real vehicles, in this case quadrotors. To test the concept in simulation a trajectory tracking controller is designed and a model of the plant derived. Finally, results of experimental tests are presented demonstrating the performance of the proposed solution for autonomous vehicle motion coordination.

I. Introduction

The problem of robot coordination poses an important challenge to automatic control. It has been the scope of a number of publications and experimental results are beginning to appear [1]–[7].

Robot coordination have proven to be advantageous in carrying out a variety of tasks such as surveillance and area exploration [2], where it results in a faster and more efficient process, or load transportations [3], where the employment of multiple robots allows for the use of smaller vehicles.

Several methodologies for coordinated motion have been developed over the past 15 years. Most of them employ the concept of artificial potentials to control the robot constellation. One such example is the work developed in [4]. With that strategy it is possible to control the shape and orientation of the formation by proper positioning some of the vehicles, called virtual leaders, although generating their trajectories may be difficult. Other strategies making use of artificial potentials may be found in [5] and [6]. However, these later strategies do not enforce a definite vehicle configuration, only driving the vehicles to fixed distances relative to each other.

In contrast to the foregoing strategies, which might be used as higher level controllers for the vehicle formation, generating trajectories to be tracked by lower level controllers, it is possible to design integrated controllers that act directly on each plant inputs to promote vehicle formation. Such concept is developed for a group of quadrotors in [7]. The development of this type of approach is more complex as it is necessary to take into account the dynamical model of the vehicles, instead of using a simpler model. Furthermore it cannot be applied to other types of vehicles as the control law is specific to the model considered.

The strategy for coordinated movement presented in this paper separates the coordination part from the control of each vehicle. A trajectory planner is responsible for generating trajectories that are tracked by the vehicles, in the present case, quadrotors. The trajectories are generated based solely on the movement of the leader, also a quadrotor, which is describing a pre-assigned trajectory unknown to the followers.

The constrained motion of the followers allows for the generation of valid formation trajectories by simply guaranteeing that the position of the leader in the reference frame of each follower converges to a desired constant vector.

The trajectory planner consists of a group of virtual vehicles (virtual followers) trying to follow the leader and whose trajectories are used as reference to the real vehicles. In contrast to the strategies proposed in [4], [5], and [6], where vehicles are modelled as point particles, the nonholonomic model of the unicycle is used to model the virtual vehicles.

Each virtual vehicle is controlled using a law developed according to the backstepping procedure. Backstepping is a well known technique extensively used for control of nonlinear systems (see for example [8]). Although backstepping is not normally applicable to underactuated systems, writing the errors in terms of the body frame allowed to concentrate the control inputs in one vector.

For the purpose of testing in simulation the concept for coordination applied to quadrotors, a trajectory tracking controller was designed using a backstepping procedure similar to what is described in [9]. The main difference is the introduction of a saturation in the contribution of both position and velocity errors to the subsequent steps of backstepping. This saturation ensures that the actuation does not grow unbounded with the errors.

This paper is structured in V sections. Section II contains a description and simulated results of the designed strategy for coordinated movement. Section III presents the developed concept to flight coordination applied to quadrotors. The plant model is described and a control law for trajectory tracking is described. Also simulated results are included. Section IV contains the experimental part of the work. The set-up is described and results are presented and discussed. The last section (section V) summarises the content of this paper.

II. Trajectory Planner

Consider a two-dimensional world where a group of followers tries to follow a leader whose movement is known up to the second derivative $\{\mathbf{p}_L, \dot{\mathbf{p}}_L, \ddot{\mathbf{p}}_L\}$. The objective of the vehicles is to move in such a way as to 'see' the leader always in the same relative position.

Each follower moves independently of its peers. Thus, for most of the coming description a generic follower is used.

A. Vehicle Model

The followers are modelled as nonholonomic vehicles that can move forward and backward and rotate but cannot move sideways and do not slip. Such vehicle is similar to a four wheeled car whose wheels can move independently in pairs but cannot steer (see figure 1).

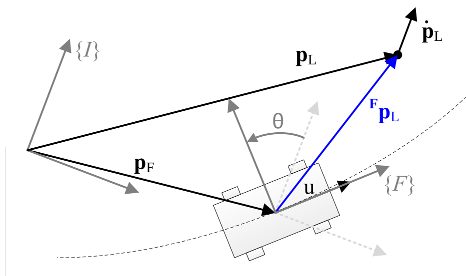

Figure 1. Illustration of the vehicle moving in the 2D-Space.

Consider the use of two different frames: a fixed inertial frame $\{I\}$, and a frame $\{F\}$, attached to the follower vehicle geometric centre and with the first vector of the basis aligned with the vehicle's direction of movement. The configuration of $\{F\}$ with respect to $\{I\}$, can be expressed using an element of the special euclidean group, $(\mathcal{R}, \mathbf{p}_F) = \left({}^I_F\mathbf{R}, {}^I\mathbf{p}_F\right) \in SE(2)$. The matrix $\mathcal{R}$ may be parametrised with an angle θ, representing the angular displacement between the two frames.

$$\mathcal{R} = \begin{bmatrix} \cos\theta & -\sin\theta \\ \sin\theta & \cos\theta \end{bmatrix} \tag{1}$$

The kinematic equations describing the motion of a follower may be written as

$$\dot{\mathcal{R}} = \mathcal{R}\mathbf{S}\left(\omega\right) \tag{2}$$
$$\dot{\mathbf{p}}_F = \mathcal{R}\mathbf{i}u \tag{3}$$

where $u \in \mathbb{R}$ and $\omega \in \mathbb{R}$ are respectively the linear and angular speeds and $\mathbf{i} = [1 \;\; 0]^T$. $\mathbf{S}\left(x\right)$ is a skew-symmetric matrix of its scalar argument. These kinematic equations completely describe the motion of the vehicle. However, in order to be possible to know the acceleration of the system, the state is extended to include the derivatives of the angular and linear speeds, respectively, which will be considered as actuations.

$$\dot{u} = T \tag{4}$$
$$\dot{\omega} = \tau \tag{5}$$

B. Controller Design

The objective of this control law is to drive the vehicle to such that the position of the leader in its frame (frame $\{F\}$) equals a desired position $\mathbf{d}$, i.e.

$$^F\mathbf{p}_L = \mathcal{R}^T\left(\mathbf{p}_L - \mathbf{p}_F\right) = \mathbf{d} \tag{6}$$

Let a position error be defined as

$$\mathbf{e}_1 = {}^F\mathbf{p}_L - \mathbf{d} \tag{7}$$

and consider a first Lyapunov candidate function given by

$$V_1 = \frac{1}{2}\mathbf{e}_1^T\mathbf{e}_1 \tag{8}$$

Computing the time derivative of V_1 yields

$$\begin{aligned} \dot{V}_1 =& \mathbf{e}_1^T\dot{\mathbf{e}}_1 \\ =& \mathbf{e}_1^T\left[-\mathbf{S}(\omega)^F\mathbf{p}_L + \mathcal{R}^T\dot{\mathbf{p}}_L - u\mathbf{i}\right] \\ =& \mathbf{e}_1^T\left[-\mathbf{S}(\omega)\left(\mathbf{e}_1 + \mathbf{d}\right) + \mathcal{R}^T\dot{\mathbf{p}}_L - u\mathbf{i}\right] \\ =& \mathbf{e}_1^T\left[-\mathbf{S}(\omega)\mathbf{d} + \mathcal{R}^T\dot{\mathbf{p}}_L - u\mathbf{i}\right] \\ =& -k_1\mathbf{e_1}^T\boldsymbol{\sigma}(\mathbf{e_1}) \\ &+ k_1\mathbf{e_1}^T\left[\boldsymbol{\sigma}(\mathbf{e_1}) + \frac{1}{k_1}\left(-\mathbf{S}(\omega)\mathbf{d} + \mathcal{R}^T\dot{\mathbf{p}}_L - u\mathbf{i}\right)\right] \end{aligned} \tag{9}$$

Notice that $\mathbf{e}_1^T\mathbf{S}(\omega)\mathbf{e}_1$ was removed from the equation using the mathematical property $\mathbf{a}^T\mathbf{S}\left(b\right)\mathbf{a} = 0$. The term $\boldsymbol{\sigma}(.)$ is a sigmoidal saturation function, applied element wise, which is introduced to limit the influence of the position error on the actuation and is given by

$$\boldsymbol{\sigma}(\mathbf{e_1}) = p_{\max}\tanh\left(\mathbf{x}/p_{\max}\right) \tag{10}$$

where $p_{\max}$ is a configurable parameter.

Following the backstepping procedure, a new error is created and the Lyapunov candidate function extended to include it.

$$\mathbf{e}_2 = \boldsymbol{\sigma}(\mathbf{e_1}) + \frac{1}{k_1}\left(-\mathbf{S}(\omega)\mathbf{d} + \mathcal{R}^T\dot{\mathbf{p}}_L - u\mathbf{i}\right) \tag{11}$$

$$V_2 = \frac{1}{2}\sum_{i=1}^{2}\mathbf{e_i}^T\mathbf{e_i} \tag{12}$$

The time derivative of V_2 is given by

$$\begin{aligned} \dot{V}_2 =& \dot{V}_1 + \mathbf{e}_2^T\dot{\mathbf{e}}_2 \\ =& \dot{V}_1 + \mathbf{e}_2^T\dot{\boldsymbol{\sigma}}(\mathbf{e_1}) \\ &- \frac{\mathbf{e}_2^T}{k_1}\left(\mathbf{S}\left(\tau\right)\mathbf{d} + \mathbf{S}(\omega)\mathcal{R}^T\dot{\mathbf{p}}_L - \mathcal{R}^T\ddot{\mathbf{p}}_L + \mathbf{i}T\right) \\ =& \dot{V}_1 + \mathbf{e}_2^T\dot{\boldsymbol{\sigma}}(\mathbf{e_1}) \\ &- \frac{\mathbf{e}_2^T}{k_1}\left(\begin{bmatrix} 1 & -d_y \\ 0 & d_x \end{bmatrix}\begin{bmatrix} T \\ \tau \end{bmatrix} + \mathbf{S}(\omega)\mathcal{R}^T\dot{\mathbf{p}}_L - \mathcal{R}^T\ddot{\mathbf{p}}_L\right) \end{aligned} \tag{13}$$

The algebraic manipulation carried out in the last step concentrated the vehicle's actuation in only one vector, multiplied by a constant matrix, which is invertible provided that $d_x \neq 0$. Defining

$$\boldsymbol{\Gamma} = \begin{bmatrix} 1 & -d_y \\ 0 & d_x \end{bmatrix} \tag{14}$$

$$\boldsymbol{\mu} = \begin{bmatrix} T \\ \tau \end{bmatrix} \tag{15}$$

$$\boldsymbol{\delta} = -\mathbf{S}(\omega)\mathcal{R}^T\dot{\mathbf{p}}_L + \mathcal{R}^T\ddot{\mathbf{p}}_L \tag{16}$$

$\dot{V}_2$ can be rewritten as

$$\dot{V}_2 = \dot{V}_1 + \frac{\mathbf{e}_2^T}{k_1}\left(k_1\dot{\boldsymbol{\sigma}}(\mathbf{e_1}) + \boldsymbol{\delta} - \boldsymbol{\Gamma}\boldsymbol{\mu}\right) \tag{17}$$

To force the convergence of the errors even in the presence of any perturbation, an integral state is introduced.

$$\dot{\boldsymbol{\xi}} = \mathbf{e}_2 \tag{18}$$

Consider a new Lyapunov candidate function given by

$$V_3 = V_2 + \frac{k_3}{2}\boldsymbol{\xi}^T\boldsymbol{\xi} \tag{19}$$

The time derivative of V_3 is given by

$$\begin{aligned}\dot{V}_3 =& \dot{V}_2 + k_3\boldsymbol{\xi}^T\mathbf{e}_2 \\ =& \dot{V}_1 + \frac{\mathbf{e}_2^T}{k_1}\left(k_1\dot{\boldsymbol{\sigma}}(\mathbf{e_1}) + \boldsymbol{\delta} + k_1k_3\boldsymbol{\xi} - \boldsymbol{\Gamma}\boldsymbol{\mu}\right)\end{aligned} \tag{20}$$

As a control law for $\boldsymbol{\mu}$, consider

$$\boldsymbol{\mu} = \Gamma^{-1}\left(\boldsymbol{\delta} + k_1\dot{\boldsymbol{\sigma}}(\mathbf{e_1}) + k_1^2k_2\mathbf{e}_2 + k_1k_3\boldsymbol{\xi}\right) \tag{21}$$

which is well defined for any $d_x \neq 0$. At this point, it is possible to state the following result.

Theorem 1. *Consider the simplified vehicle model described in equations* (2)-(5) *and the error system consisting of the errors* $\mathbf{e}_1$ (7) *and* $\mathbf{e}_2$ (11). *The control law* (21) *with* $k_1 > 0$, $k_2 > 1$, *and* $k_3 > 0$, *renders the origin of the error system globally asymptotically stable.*

Proof: Substituting $\boldsymbol{\mu}$, $\dot{\mathbf{e}}_2$ becomes

$$\dot{\mathbf{e}_2} = -\boldsymbol{\Gamma}\boldsymbol{\mu} + \boldsymbol{\delta} + \dot{\boldsymbol{\sigma}}(\mathbf{e_1}) = -k_1k_2\mathbf{e}_2 - k_1k_3\boldsymbol{\xi}$$

and the system of equations for $\mathbf{e}_2$ and $\boldsymbol{\xi}$ can be written as

$$\dot{\mathbf{x}} = \begin{bmatrix}\dot{\boldsymbol{\xi}} \\ \dot{\mathbf{e}_2}\end{bmatrix} = -\begin{bmatrix}0 & -1 \\ k_1k_3 & k_1k_2\end{bmatrix}\begin{bmatrix}\boldsymbol{\xi} \\ \mathbf{e}_2\end{bmatrix} \tag{22}$$

For k_1, k_2, and $k_3 > 0$, the origin of (22) is globally exponentially stable, which implies that there exist positive scalars λ and α such that

$$\|\mathbf{x}\| \leq \alpha\|\mathbf{x}(0)\|e^{-\lambda t}$$

To prove that the origin is asymptotically stable consider the substitution of equation (21) into (13) yielding

$$\begin{aligned}\dot{V}_3 =& -k_1\mathbf{e}_1^T\boldsymbol{\sigma}(\mathbf{e_1}) + k_1\mathbf{e}_1^T\mathbf{e}_2 - k_1k_2\mathbf{e}_2^T\mathbf{e}_2 \\ \leq& -k_1\|\mathbf{e}_1\|\|\boldsymbol{\sigma}(\mathbf{e_1})\| + k_1\|\mathbf{e}_1\|\|\mathbf{e}_2\| - k_1k_2\|\mathbf{e}_2\|^2\end{aligned}$$

which is negative whenever either $\|\mathbf{e}_2\| \leq \|\boldsymbol{\sigma}(\mathbf{e_1})\|$ or $\|\mathbf{e}_1\| \leq k_2\|\mathbf{e}_2\|$ is verified. If $k_2 > 1$, then there exists $\|\mathbf{e}_1\| > 0$ for which $\|\mathbf{e}_1\| = k_2\|\sigma(\mathbf{e}_1)\| = k_2c$. When $\|\mathbf{e}_2\| \leq c$, $\dot{V}_3$ becomes negative definite.

Since $\|\mathbf{e}_2\| \leq \|\mathbf{x}\| \leq \alpha\|\mathbf{x}(0)\|e^{-\lambda t}$, there is a time t_1 when, for $t > t_1$, $\dot{V}_3$ becomes negative semi-definite. Since the error systems is autonomous, we can apply LaSalle's Invariance Principle to conclude that the origin is globally asymptotically stable. ■

C. Inner Dynamics Analysis

Having the error system stable does not imply that the intrinsic variables of the vehicle are stable. For a given leader's position and a given $\mathbf{d}$ there are infinite solutions satisfying the condition (6) which indicates the existence of a zero dynamics , whose stability needs to be analysed. Towards that end, consider the limit condition when the errors have converged to zero. In that situation it is possible to write:

$$\begin{bmatrix}u \\ \dot{\theta}\end{bmatrix} = \boldsymbol{\Gamma}^{-1}\mathcal{R}^T\dot{\mathbf{p}}_L \tag{23}$$

Let us define $\dot{\mathbf{p}}_L$ as

$$\dot{\mathbf{p}}_L = V_L\begin{bmatrix}\cos\theta_L \\ \sin\theta_L\end{bmatrix} \tag{24}$$

with V_L and θ_L continuous functions representing the norm and direction of movement of the leader, respectively. Using these definitions, equation (23) can be rearranged into the form

$$\begin{bmatrix}u \\ \dot{\theta}\end{bmatrix} = \begin{bmatrix}V_L\cos(\theta_L - \theta) + \dfrac{V_Ld_y}{d_x}\sin(\theta_L - \theta) \\ \dfrac{V_L}{d_x}\sin(\theta_L - \theta)\end{bmatrix} \tag{25}$$

It is worth noting that the second equation has solely one variable, θ (apart from the inputs), and that it does not depend on d_y.

Applying the change of variables $\theta_d = \theta - \theta_L$, the zero-dynamics can be written as

$$\dot{\theta}_d = -\frac{V_L}{d_x}\left(\sin\theta_d + d_x\kappa_L\right) \tag{26}$$

where $\kappa_L = \omega_L/V_L$ is the curvature of the leader's path.

The analysis that follows is divided in two cases: a) trajectories with $\dot{\kappa}_L = 0$; and b) trajectories with $\dot{\kappa}_L \neq 0$.

For $\dot{\kappa}_L = 0$: Trajectories with $\dot{\kappa}_L = 0$ can be either a circumference, when $\kappa_L \neq 0$, or a line, otherwise. For this type of trajectories it is possible to prove stability. Towards that end consider the candidate Lyapunov function

$$V_\theta = \frac{1}{2}\left(\sin\theta_d + d_x\kappa_L\right)^2 \tag{27}$$

whose time derivative is given by

$$\begin{aligned}\dot{V}_\theta =& \left(\sin\theta_d + d_x\kappa_L\right)\left(\cos\theta_d\dot{\theta}_d + d_x\dot{\kappa}_L\right) \\ =& -\frac{V_L}{d_x}\cos\theta_d\left(\sin\theta_d + d_x\kappa_L\right)^2 = -2\frac{V_L}{d_x}\cos\theta_d\, V_\theta\end{aligned}$$

which is zero for $\theta_d = \pm\pi/2$ and for $\sin\theta_d = -d_x\kappa_L$. Analysing the stability of these points it can be seen that only

$$\theta_d = -\arcsin(d_x\kappa_L) \tag{28}$$

corresponds to a stable equilibrium point. Therefore, for any pair $\{d_x, \kappa_L\}$ there is only one stable value of θ_d. It can also be seen that no stable solution can be found for $d_x\kappa_L > 1$. Such situation is equivalent to having d_x greater than the circumference radius, $d_x > \kappa_L^{-1}$.

For $\dot{\kappa}_L \neq 0$: When the trajectory being tracked has a time-varying curvature the analysis is more difficult. However, analysing equation (26) it is possible to conclude the following:

- when $d_x\kappa_L \mapsto 0$, $\dot{\theta}_d \approx -\frac{V_L}{d_x}\sin\theta_d$ which means that $\theta_d \mapsto 0$. Since $\theta = \theta_d + \theta_L$, θ will approach θ_L which means that the movement of the follower will be similar to the leader's.
- when $d_x\kappa_L \mapsto \infty$, $\dot{\theta}_d \approx -\omega_L$. In such situation $\theta_d \approx -\theta_L + c$, where c is a constant that depends on the initial conditions. Writing this result in terms of θ, one sees that $\theta \mapsto c$. This result indicates that, for large values of d_x, θ is slow varying. As one can imagine, if the follower is far way from the leader it does not have to move much in order to 'see' the leader in the same position.

This limit analysis indicates that, for intermediate values of $d_x\kappa_L$ a trade-off between these two behaviours is to be expected. When the value of $d_x\kappa_L$ is small, the movement of a follower resembles the one described by the leader. On the other hand, as $d_x\kappa_L$ grows, the differences between the trajectory described by the leader and the one described by a follower intensify until the motion of the later starts depending on its initial conditions. It is therefore of interest to find limits on the parameters prevent such behaviour.

Rewriting the first part of equation (25) as

$$\frac{u}{V_L} = \cos\theta_d - \frac{d_y}{d_x}\sin\theta_d$$

one sees that u depends only on V_L and θ_d. In particular, one sees that, for small values of θ_d, the minimum value of u/V_L corresponds to the maximum value of the former

$$\left.\frac{u}{V_L}\right|_{\min} = \cos|\theta_d|_{\max} - \left|\frac{d_y}{d_x}\right|\sin|\theta_d|_{\max}$$

For the movement of a follower to be similar to the movement of the leader no inversion in the direction of movement of the former may occur, which means

$$0 = \cos\theta_d - \frac{d_y}{d_x}\sin\theta_d \Leftrightarrow \tan\theta_d = \frac{d_x}{d_y}$$

may never be verified, which is guaranteed if

$$|\theta_d|_{\max} < \arctan|d_x/d_y| \tag{29}$$

From evaluation of equation (26) we see that

$$|\theta_d|_{\max} = \arcsin\left(d_x\ \kappa_L|_{\theta_{d\max}}\right) \leq \arcsin|d_x\kappa_L|_{\max} \tag{30}$$

which is a bound for θ_d. Having $\arcsin d_x\kappa_{L\max} < \arctan|d_x/d_y|$ guarantees that no inversion occurs. This condition can be used to, given $\mathbf{d}$, set limits on the trajectory the leader can describe and vice-versa.

D. Simulation Results

This sub-section presents the results of a simulation for the generation of a formation trajectory where two virtual vehicles were set to follow a leader describing a trajectory given by

$$\mathbf{p}_{ref} = \begin{bmatrix} 2\cos(0.25t) \\ \sin(0.5t) \end{bmatrix} \tag{31}$$

Follower 1 has $\mathbf{d}_1 = [0.35\ 0.35]^T$ and its initial state is $\mathbf{p}_{F1}(0) = [3\ 3]^T$, $u_{F1}(0) = 0.5$, $\omega_{F1}(0) = -0.5$, $\theta_{F1}(0) = 3\pi/2$. Follower 2 has $\mathbf{d}_2 = [0.35\ \ -0.35]^T$, $\mathbf{p}_{F2}(0) = [3\ 1]^T$, $u_{F2}(0) = 0$, $\omega_{F2}(0) = 0.5$, $\theta_{F2}(0) = 0$. The controller parameters are $k_1 = 0.2$, $k_2 = 2$, $k_3 = 0$, and $p_{\max} = 5$.

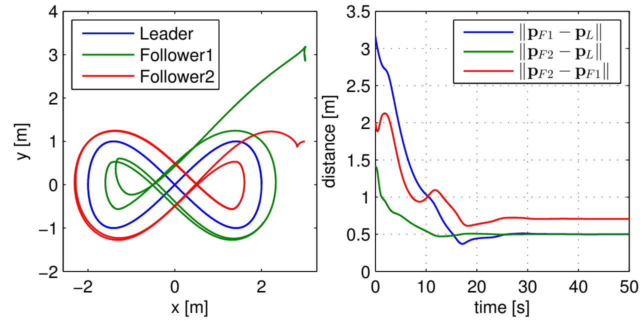

Figure 2. Position (L) and distance between vehicles (R) during a simulation.

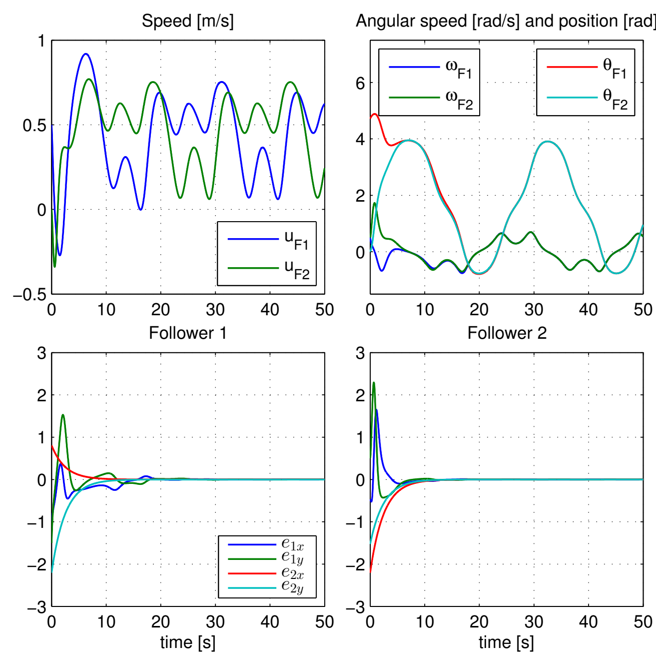

Figure 3. Followers states (T) and errors (B) during a simulation.

Although the trajectories of both followers are different (figure 2 left), their angular speed and position converge to one another. This is in accordance with the analysis made in subsection II-C, where it was concluded that these variables do not depend on d_y, the only parameter that is different between followers in this simulation.

The right image of figure 2 indicates that the distance between followers and between these and the leader converge to fixed values. The later is a direct implication of the asymptotic stability of the error system. The former, the distance between followers, is a result of the independence of each follower's u, ω and θ from d_y. The limit to which this distance converges is equal to the sum of the followers distance, in this case $0.35 + 0.35 = 0.7\text{m}$. These results indicate that, a formation where all the followers have the same value of d_x is asymptotically a rigid formation.

E. Three-dimensional trajectories

So far only two-dimensional motion has been considered. However, to generate trajectories for quadrotors it is necessary to consider three-dimensional motion. Instead of deriving a law for the entire state space, a separate control law is designed to drive the vertical coordinate of the virtual follower to a desired distance to the leader. Consider that the desired vectorial distance $\mathbf{d}$ is extended to include a third component d_z and let e_z be the vertical position error given by

$$e_z = p_{Lz} - p_{Fz} - d_z \tag{32}$$

A simple control law that stabilises e_z, might be

$$\ddot{p}_{Fz} = \sigma_z \left(\ddot{p}_{Lz} + k_{z1}e_z + k_{z2}\dot{e}_z\right) \tag{33}$$

where, $\sigma_z(x)$ is given by

$$\sigma_z(x) = \begin{cases} x & \text{if } |x| < z_{\max} \\ \text{sign}(x)z_{\max} & \text{if } |x| > z_{\max} \end{cases} \tag{34}$$

This saturation is introduced to protect the followers from any unexpected acceleration of the leader. The control law guarantees asymptotic stability of e_z if the condition $\ddot{\mathbf{p}}_{Lz} < z_{\max}$ is verified.

The equations that govern the trajectory generation are summarised as follows

$$\ddot{\mathbf{p}}_F = \begin{bmatrix} \mathcal{R}\mathbf{S}(\omega)\mathbf{i}u + \mathcal{R}\mathbf{i}T \\ \sigma_z\left(\ddot{p}_{Lz} + k_{z1}e_z + k_{z2}\dot{e}_z\right) \end{bmatrix} \tag{35}$$

$$\dot{\mathcal{R}} = \mathcal{R}\mathbf{S}(\omega) \tag{36}$$

$$\dot{u} = T \tag{37}$$

$$\dot{\omega} = \tau \tag{38}$$

$$\begin{bmatrix} T \\ \tau \end{bmatrix} = \Gamma^{-1}\left(\delta + k_1\dot{\boldsymbol{\sigma}}(\mathbf{e_1}) + k_1^2k_2\mathbf{e}_2 + k_1k_3\boldsymbol{\xi}\right) \tag{39}$$

As was observed in simulation, during the formation initialisation inversions in the direction of movement of the virtual followers are likely to occur. To prevent the following vehicles from being affected the virtual followers are started at their intended initial positions. Using information from the reference trajectory of the leader, the virtual followers are placed initially with null errors with respect to the reference trajectory, and oriented in the initial planar direction of the reference trajectory, i.e. the normalised projection of the reference velocity at t = 0.

Until both the leader and follower vehicles approach the initial reference and virtual followers, respectively, the controllers of the virtual vehicles are turned off. Once that happens these controllers are turned on and the leader starts tracking the reference trajectory. The start of the tracking is triggered when the positional errors of every quadrotor enter a set $\mathbf{e}_1 < e_{\max}$ ($\mathbf{e}_1$ defined in next section)

$$\begin{aligned} trigger = &(\|\mathbf{e}_{1L}\| < e_{\max}) \wedge (\|\mathbf{e}_{1F_1}\| < e_{\max}) \wedge \\ &\wedge \cdots \wedge (\|\mathbf{e}_{1F_n}\| < e_{\max}) \end{aligned} \tag{40}$$

III. Quadrotors in Formation

A. Quadrotor model

The quadrotor is modelled as a rigid body that is actuated in force and torque. Consider a fixed inertial frame $\{I\}$ and another frame $\{B\}$ attached to the vehicle's centre of mass. The configuration of the body frame $\{B\}$ with respect to $\{I\}$ can be viewed as an element of the Special Euclidean group, $(\mathbf{R}, \mathbf{p}) = ({}^I_B\mathbf{R}, {}^I\mathbf{p}_B) \in SE(3)$. The kinematic and dynamic equations of motion for the rigid body can be written as

$$\dot{\mathbf{R}} = \mathbf{R}\mathbf{S}(\boldsymbol{\omega}) \tag{41}$$

$$\dot{\mathbf{p}} = \mathbf{R}\mathbf{v} \tag{42}$$

$$\dot{\mathbf{v}} = -\mathbf{S}(\boldsymbol{\omega})\mathbf{v} + \frac{1}{m}\mathbf{f}_{ext} \tag{43}$$

$$\dot{\boldsymbol{\omega}} = -\mathbf{J}^{-1}\mathbf{S}(\boldsymbol{\omega})\mathbf{J}\boldsymbol{\omega} + \mathbf{J}^{-1}\mathbf{m}_{ext} \tag{44}$$

In the foregoing equations, $\boldsymbol{\omega} \in \mathbb{R}^3$ and $\mathbf{v} \in \mathbb{R}^3$ denote the angular and linear velocities and vectors $\mathbf{f}_{ext}$ and $\mathbf{m}_{ext}$ represent the external forces and moments acting on the vehicle, respectively, all expressed in the body frame. $\mathbf{S}(.)$ is a skew symmetric matrix of its argument verifying $\mathbf{S}(\mathbf{a})\mathbf{b} = \mathbf{a} \times \mathbf{b}$, for any $\mathbf{a}$ and $\mathbf{b} \in \mathbb{R}^3$. Lastly, m is the mass of the vehicle and $\mathbf{J}$ its tensor of inertia.

The most commonly adopted model for quadrotors (e.g. [9]) consider that torques can be generated in any direction and that the only actuation force is the thrust T, aligned with the body's vertical axis. The external force is then given by

$$\mathbf{f}_{ext} = -T\mathbf{k} + mg\mathbf{R}^T\mathbf{k} \tag{45}$$

where $\mathbf{k} = [0\ 0\ 1]^T$ and g is the gravitational acceleration. As the plant has full torque actuation, the input transformation

$$\mathbf{m}_{ext} = \mathbf{J}\boldsymbol{\tau} + \mathbf{S}(\boldsymbol{\omega})\mathbf{J}\boldsymbol{\omega} \tag{46}$$

can be used to reduce equation (44) to an integrator form

$$\dot{\boldsymbol{\omega}} = \boldsymbol{\tau} \tag{47}$$

From equations (45) and (46) one sees that the quadrotor has only 4 actuation variables for 6 degrees of freedom, being an underactuated vehicle.

B. Quadrotor trajectory tracking controller

Let the desired trajectory be given by $\mathbf{p}_d(t) \in \mathbb{R}^3$, a function of time and at least of class C^4. In the sequel, time dependence will be omitted to lighten notation. The procedure that follows consists in deriving a control law for the thrust associated to the concepts of desired thrust and desired thrust direction. From that point onwards backstepping is used until unveiling the other control inputs.

Consider the position error $\mathbf{e}_1$ given by

$$\mathbf{e}_1 = \mathbf{p} - \mathbf{p}_d \tag{48}$$

and the velocity error which equals $\dot{\mathbf{e}}_1$

$$\mathbf{e}_2 = \dot{\mathbf{e}}_1 = \mathbf{R}\mathbf{v} - \dot{\mathbf{p}}_d \tag{49}$$

The time derivative of $\mathbf{e}_2$ is given by

$$\begin{aligned}\dot{\mathbf{e}}_2 =& \ddot{\mathbf{e}}_1 = \frac{1}{m}\mathbf{Rf} - \ddot{\mathbf{p}}_d = -\frac{T}{m}\mathbf{Rk} + g\mathbf{k} - \ddot{\mathbf{p}}_d \\ =& -\boldsymbol{\sigma}_e(k_1\mathbf{e}_1 + k_2\mathbf{e}_2) \\ &+ \left(-\frac{T}{m}\mathbf{Rk} + g\mathbf{k} - \ddot{\mathbf{p}}_d + \boldsymbol{\sigma}_e(k_1\mathbf{e}_1 + k_2\mathbf{e}_2)\right)\end{aligned}$$

where $\boldsymbol{\sigma}_e(\cdot)$ is an element wise saturation function introduced to limit the influence of errors $\mathbf{e}_1$ and $\mathbf{e}_2$ in the actuation and is given by

$$\boldsymbol{\sigma}_e(\mathbf{x}) = \sigma_{\max}\frac{x_i}{\sqrt{c + x_i^2}} \tag{50}$$

where $\sigma_{\max}$ and c are configurable parameters. Henceforth, the dependence of $\boldsymbol{\sigma}_e$ on $k_1\mathbf{e}_1 + k_2\mathbf{e}_2$ is omitted for lighter notation.

Let T_d and $\mathbf{r}_{3d}$ be the desired thrust and desired thrust direction, respectively, given by

$$T_d = m\|g\mathbf{k} - \ddot{\mathbf{p}}_d + \boldsymbol{\sigma}_e\| \tag{51}$$

$$\mathbf{r}_{3d} = \frac{g\mathbf{k} - \ddot{\mathbf{p}}_d + \boldsymbol{\sigma}_e}{\|g\mathbf{k} - \ddot{\mathbf{p}}_d + \boldsymbol{\sigma}_e\|} \tag{52}$$

The desired thrust direction is not well defined for $T_d = 0$. To guarantee that T_d remains positive the limits of $\boldsymbol{\sigma}_e$ must be chosen carefully. Concentrating on the third component of $\mathbf{r}_{3d}$ and recalling that, by equation (33), $|\mathbf{k}^T\ddot{\mathbf{p}}_d|$ is limited to $z_{\max}$, an upper limit to $\sigma_{\max}$ is given by

$$\sigma_{\max} < g - z_{\max} \tag{53}$$

Using this saturation, $T_d = 0$ is never be verified.

At this point, consider a control law for the thrust given by

$$T = \mathbf{r}_{3d}^T\mathbf{r}_3 T_d \tag{54}$$

Substitution of (54) into $\dot{\mathbf{e}}_2$ allows it to be rewritten as

$$\begin{aligned}\dot{\mathbf{e}}_2 =& -\boldsymbol{\sigma}_e + \frac{1}{m}\left(T_d\mathbf{r}_{3d} - T\mathbf{r}_3\right) \\ =& -\boldsymbol{\sigma}_e - \frac{T_d}{m}\mathbf{S}(\mathbf{r_3})^2\mathbf{r}_{3d}\end{aligned}$$

Consider a Lyapunov candidate function V_σ given by

$$V_\sigma = \frac{1}{2}\begin{bmatrix}\boldsymbol{\sigma}_e^T & \mathbf{e}_2^T\end{bmatrix}\mathbf{P}\begin{bmatrix}\boldsymbol{\sigma}_e \\ \mathbf{e}_2\end{bmatrix} + \sum_{i=x,y,z}\int_0^{k_1 e_{1i} + k_2 e_{2i}} \sigma_e(u)du \tag{55}$$

where $\mathbf{P}$ is a constant, symmetric and positive definite matrix given by

$$\mathbf{P} = \begin{bmatrix} p_{11}\mathbf{I}_3 & -p_{12}\mathbf{I}_3 \\ -p_{12}\mathbf{I}_3 & p_{22}\mathbf{I}_3\end{bmatrix} \tag{56}$$

with $p_{11}, p_{22} > 0$ and $p_{12}^2 < p_{11}p_{22}$ and where $\mathbf{I}_3$ represents the identity matrix. The first term of (55) is quadratic and thus positive. The second term is the integral of a monotonically increasing function, which is also positive. Therefore (55) is a positive function. Computing the time derivative of V yields

$$\begin{aligned}\dot{V}_\sigma =& \begin{bmatrix}\boldsymbol{\sigma}_e^T & \mathbf{e}_2^T\end{bmatrix}\mathbf{P}\begin{bmatrix}\dot{\boldsymbol{\sigma}}_e \\ \dot{\mathbf{e}}_2\end{bmatrix} + \boldsymbol{\sigma}_e^T \cdot (k_1\dot{\mathbf{e}}_1 + k_2\dot{\mathbf{e}}_2) \\ =& \begin{bmatrix}\boldsymbol{\sigma}_e^T & \mathbf{e}_2^T\end{bmatrix}\mathbf{P}\begin{bmatrix}\boldsymbol{\sigma}_e' \cdot (k_1\dot{\mathbf{e}}_1 + k_2\dot{\mathbf{e}}_2) \\ -\boldsymbol{\sigma}_e - \frac{T_d}{m}\mathbf{S}(\mathbf{r_3})^2\mathbf{r}_{3d}\end{bmatrix} \\ &+ \boldsymbol{\sigma}_e \cdot \left[k_1\mathbf{e}_2 - k_2\left(\boldsymbol{\sigma}_e + \frac{T_d}{m}\mathbf{S}(\mathbf{r_3})^2\mathbf{r}_{3d}\right)\right]\end{aligned}$$

The apostrophe on $\boldsymbol{\sigma}_e'$ denotes the partial derivative of $\boldsymbol{\sigma}_e$ with respect to its argument, $\frac{\partial}{\partial\mathbf{x}}\boldsymbol{\sigma}_e(\mathbf{x})$, which is a diagonal matrix, since the saturation function is element wise. Some mathematical manipulation allows $\dot{V}_\sigma$ do be rewritten in the form

$$\dot{V}_\sigma = -\begin{bmatrix}\boldsymbol{\sigma}_e^T & \mathbf{e}_2^T\end{bmatrix}\mathbf{Q}\begin{bmatrix}\boldsymbol{\sigma}_e \\ \mathbf{e}_2\end{bmatrix} - \boldsymbol{\delta}\left(\mathbf{e}_1, \mathbf{e}_2\right)^T\frac{T_d}{m}\mathbf{S}(\mathbf{r_3})^2\mathbf{r}_{3d} \tag{57}$$

where,

$$\boldsymbol{\delta}\left(\mathbf{e}_1, \mathbf{e}_2\right) = k_2\boldsymbol{\sigma}_e'\left(p_{11}\boldsymbol{\sigma}_e - p_{12}\mathbf{e}_2\right) + \left(k_2 - p_{12}\right)\boldsymbol{\sigma}_e + p_{22}\mathbf{e}_2 \tag{58}$$

and $\mathbf{Q}$ is a block matrix composed by

$$\begin{aligned}\mathbf{Q}_{11} &= (k_2 - p_{12})\mathbf{I}_3 + p_{11}k_2\boldsymbol{\sigma}_e' \\ \mathbf{Q}_{12} &= \mathbf{Q}_{21} = -\frac{k_1p_{11} + k_2p_{12}}{2}\boldsymbol{\sigma}_e' - \frac{k_1 - p_{22}}{2}\mathbf{I}_3 \\ \mathbf{Q}_{22} &= p_{12}k_1\boldsymbol{\sigma}_e'\end{aligned}$$

With a proper choice of gains and coefficients of $\mathbf{P}$, matrix $\mathbf{Q}$ can be made positive definite. Choosing $k_1 = p_{22}$ and $k_2 = p_{11}p_{22}/p_{12}$, $\mathbf{Q}$ becomes

$$\mathbf{Q} = \begin{bmatrix}\frac{p_{11}p_{22} - p_{12}^2}{p_{12}}\mathbf{I}_3 + \frac{p_{11}^2p_{22}}{p_{12}}\boldsymbol{\sigma}_e' & -p_{22}p_{11}\boldsymbol{\sigma}_e' \\ -p_{22}p_{11}\boldsymbol{\sigma}_e' & p_{12}p_{22}\boldsymbol{\sigma}_e'\end{bmatrix} \tag{59}$$

Since $\mathbf{Q}$ is a block matrix, its determinant is given by

$$\begin{aligned}\det\left(\mathbf{Q}\right) =& \det(\mathbf{Q}_{22}) \cdot \det(\mathbf{Q}_{11} - \mathbf{Q}_{12}\mathbf{Q}_{22}^{-1}\mathbf{Q}_{21}) \\ =& \det\left(p_{12}p_{22}\boldsymbol{\sigma}_e'\right) \cdot \det\left(\frac{p_{11}p_{22} - p_{12}^2}{p_{12}}\mathbf{I}_3\right) \\ =& p_{22}(p_{11}p_{22} - p_{12}^2)\det\left(\boldsymbol{\sigma}_e'\right)\end{aligned}$$

Since $\boldsymbol{\sigma}_e$ is diagonal with positive elements, its determinant is positive. From the imposition of positive definiteness of $\mathbf{P}$ it follows that $p_{22} > 0$ and $p_{12}^2 < p_{11}p_{22}$. These conditions imply $\mathbf{Q}$ to be positive definite.

For a more compact writing consider the introduction of a positive function $W_\sigma(\mathbf{e}_1, \mathbf{e}_2)$ given by

$$W_\sigma(\mathbf{e}_1, \mathbf{e}_2) = \begin{bmatrix}\boldsymbol{\sigma}_e^T & \mathbf{e}_2^T\end{bmatrix}\mathbf{Q}\begin{bmatrix}\boldsymbol{\sigma}_e \\ \mathbf{e}_2\end{bmatrix} \tag{60}$$

Using this definition, (57) becomes

$$\dot{V}_\sigma = -W_\sigma(\mathbf{e}_1, \mathbf{e}_2) - \frac{T_d}{m}\mathbf{r}_{3d}^T\mathbf{S}(\mathbf{r_3})^2\boldsymbol{\delta}\left(\mathbf{e}_1, \mathbf{e}_2\right) \tag{61}$$

The first term of equation (61) is negative definite, whereas the second term is indefinite. To drive the second term to zero a new error is created and the candidate Lyapunov extended to include it.

$$\mathbf{e}_3 = \mathbf{r}_3 - \mathbf{r}_{3d} \tag{62}$$

$$V_3 = V_\sigma + \frac{1}{2}\mathbf{e}_3^T\mathbf{e}_3 \tag{63}$$

Computing the time derivative of V_3 yields

$$\begin{aligned}\dot{V}_3 =&\dot{V}_\sigma - \mathbf{r}_{3d}^T\dot{\mathbf{r}}_3 - \mathbf{r}_3^T\dot{\mathbf{r}}_{3d}\\ =&\dot{V}_\sigma + \mathbf{r}_{3d}^T\mathbf{R}\mathbf{S}(\mathbf{k})\left(\boldsymbol{\omega} - \mathbf{R}^T\mathbf{S}\left(\mathbf{r}_{3d}\right)\dot{\mathbf{r}}_{3d}\right)\\ =&-W_\sigma(\mathbf{e}_1,\mathbf{e}_2) - k_3\mathbf{r}_{3d}^T\mathbf{S}(\mathbf{r}_3)^T\mathbf{S}(\mathbf{r}_3)\mathbf{r}_{3d}\\ &+\mathbf{r}_{3d}^T\mathbf{R}\mathbf{S}\left(\mathbf{k}\right)\left(\boldsymbol{\omega} - \mathbf{R}^T\mathbf{S}\left(\mathbf{r}_{3d}\right)\dot{\mathbf{r}}_{3d}\right)\\ &-\mathbf{r}_{3d}^T\mathbf{R}\mathbf{S}\left(\mathbf{k}\right)^2\left(k_3\mathbf{R}^T\mathbf{r}_{3d} + \frac{T_d}{m}\mathbf{R}^T\boldsymbol{\delta}\left(\mathbf{e}_1,\mathbf{e}_2\right)\right)\\ =&-W_3(\mathbf{e}_1,\mathbf{e}_2,\mathbf{r}_3,\mathbf{r}_{3d})\\ &+\mathbf{r}_{3d}^T\mathbf{R}\mathbf{S}\left(\mathbf{k}\right)\left(\boldsymbol{\omega} - \mathbf{R}^T\mathbf{S}\left(\mathbf{r}_{3d}\right)\dot{\mathbf{r}}_{3d}\right)\\ &-\mathbf{r}_{3d}^T\mathbf{R}\mathbf{S}\left(\mathbf{k}\right)^2\left(k_3\mathbf{R}^T\mathbf{r}_{3d} + \frac{T_d}{m}\mathbf{R}^T\boldsymbol{\delta}\left(\mathbf{e}_1,\mathbf{e}_2\right)\right)\end{aligned} \tag{64}$$

where use was made of the fact that $\mathbf{S}\left(\mathbf{r}_3\right) = \mathbf{R}\mathbf{S}\left(\mathbf{k}\right)\mathbf{R}^T$.

Since the control input does not appear yet in the equation, another error $\mathbf{e}_4$ and respective Lyapunov candidate function are created.

$$\begin{aligned}\mathbf{e}_4 =&\mathbf{S}\left(\mathbf{k}\right)\left(\boldsymbol{\omega} - \mathbf{R}^T\mathbf{S}\left(\mathbf{r}_{3d}\right)\dot{\mathbf{r}}_{3d}\right)\\ &-\mathbf{S}\left(\mathbf{k}\right)^2\mathbf{R}^T\left(k_3\mathbf{r}_{3d} + \frac{T_d}{m}\boldsymbol{\delta}\left(\mathbf{e}_1,\mathbf{e}_2\right)\right)\end{aligned} \tag{65}$$

$$V_4 = V_3 + \frac{1}{2}\mathbf{e}_4^T\mathbf{e}_4 \tag{66}$$

The time derivative of V_4 gives

$$\begin{aligned}\dot{V}_4 =&\dot{V}_3 + \mathbf{e}_4^T\dot{\mathbf{e}}_4\\ =&\dot{V}_3 + \mathbf{e}_4^T\mathbf{S}\left(\mathbf{k}\right)\left(\boldsymbol{\tau} - \frac{\mathrm{d}}{\mathrm{d}t}\left\{\mathbf{R}^T\mathbf{S}\left(\mathbf{r}_{3d}\right)\dot{\mathbf{r}}_{3d}\right\}\right)\\ &-\mathbf{e}_4^T\mathbf{S}\left(\mathbf{k}\right)^2\frac{\mathrm{d}}{\mathrm{d}t}\left\{\mathbf{R}^T\left(k_3\mathbf{r}_{3d} + \frac{T_d}{m}\boldsymbol{\delta}\left(\mathbf{e}_1,\mathbf{e}_2\right)\right)\right\}\end{aligned}$$

The remaining input $\boldsymbol{\tau}$ has finally been unveiled and therefore it is now possible to write the final control law.

$$\begin{aligned}\boldsymbol{\tau} =&\mathbf{S}\left(\mathbf{k}\right)\left(k_4\mathbf{e}_4 + \mathbf{R}^T\mathbf{r}_{3d}\right) + \frac{\mathrm{d}}{\mathrm{d}t}\left\{\mathbf{R}^T\mathbf{S}\left(\mathbf{r}_{3d}\right)\dot{\mathbf{r}}_{3d}\right\} + \mathbf{k}\tau_z\\ &+\mathbf{S}\left(\mathbf{k}\right)\frac{\mathrm{d}}{\mathrm{d}t}\left\{\mathbf{R}^T\left(k_3\mathbf{r}_{3d} + \frac{T_d}{m}\boldsymbol{\delta}\left(\mathbf{e}_1,\mathbf{e}_2\right)\right)\right\}\end{aligned} \tag{67}$$

where τ_z corresponds to the third component of τ, and can be arbitrarily set. For the present controller, it was chosen to use it simply to drive ω_z to zero, and therefore

$$\tau_z = -k_z\omega_z \tag{68}$$

At this point, the result of this development is presented.

Theorem 2. *Let the quadrotor model be described by equations* (41)-(44) *and consider the control laws* (54) *and* (67). *Choosing* $k_i > 0$ *renders the origin of the error system asymptotically stable and guarantees global convergence of the tracking error to zero.*

Proof: Substitution of $\boldsymbol{\tau}$ into $\dot{V}_4$ yields

$$\dot{V}_4 = -\begin{bmatrix}\boldsymbol{\sigma}_e^T & \mathbf{e}_2^T\end{bmatrix}\mathbf{Q}\begin{bmatrix}\boldsymbol{\sigma}_e\\ \mathbf{e}_2\end{bmatrix} - k_3\mathbf{r}_{3d}^T\mathbf{S}(\mathbf{r}_3)^T\mathbf{S}(\mathbf{r}_3)\mathbf{r}_{3d} - k_4\mathbf{e}_4^T\mathbf{e}_4 \tag{69}$$

which is negative semi-definite, being negative everywhere besides the set $\{\boldsymbol{\sigma}_e = 0, \mathbf{e}_2 = 0, \mathbf{r}_3 = \pm\mathbf{r}_{3d}, \mathbf{e}_4 = 0\}$. Noting that $\boldsymbol{\sigma}_e = 0 \Rightarrow \mathbf{e}_1 + k_2\mathbf{e}_2 = 0$, having $\mathbf{e}_2 = 0$ imply $\mathbf{e}_1 = 0$. This deduction is valid for any initial conditions. Therefore, errors $\mathbf{e}_1$, $\mathbf{e}_2$, and $\mathbf{e}_4$ converge to zero for any initial conditions, meaning that trajectory tracking is achieved globally. ■

C. Simulation

The vehicles used in the simulations are all equal, weighing 0.1kg and having $I_{xx} = I_{yy} = 1 \times 10^{-3}\mathrm{kg}\cdot\mathrm{m}^2$ and $I_{yy} = 2 \times 10^{-3}\mathrm{kg}\cdot\mathrm{m}^2$. The products of inertia are assumed to be 0. These values are typical of small scale plants similar to the ones used in the experimental test of section IV. Each quadrotor controller is configured with the same parameters, being $k_1 = 0.5$, $k_2 = 1.5$, $k_3 = 10$, $k_4 = 0.5$, $k_z = 1$, $\sigma_{\max} = 5$, $c = 50$, $p_{22} = 0.5$, $p_{11} = 1$, $p_{12} = 1/3$.

Quadrotor controller test: In this simulation the quadrotor is set to track a planar trajectory described by equation (31) at a constant height $h = -1.5\mathrm{m}$. In order to demonstrate the performance of the controller, the quadrotor is initially placed at $\mathbf{p}(0) = [-5 \;\; 10 \;\; -10]^T$, with $\phi(0) = \pi$ and $\psi(0) = 0 = \theta(0)$. The velocities (linear and angular) are initially zero. This is an extremely unfavourable configuration, in which the vehicle is turned upside down. This fact causes the plant to rapidly rotate, as can be observed in figure 4 through the snapshots of the plant actuation taken at each second, or in the plot of the error $\mathbf{e}_3$ in figure 5 by the rapid evolution of the third component of the error, which indicates an inversion in direction of vector $\mathbf{r}_3$.

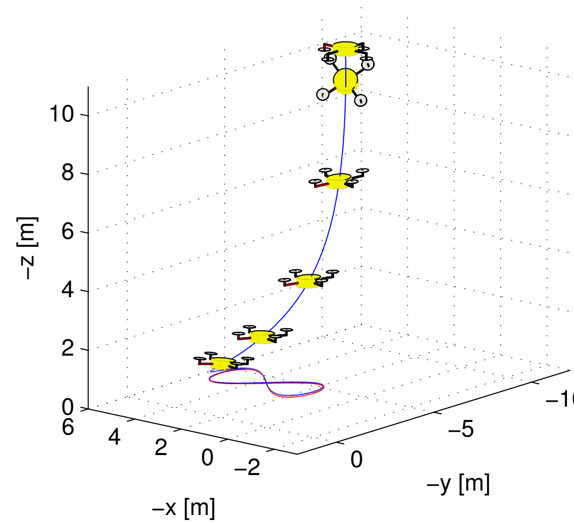

Figure 4. Trajectory described by the vehicle (blue), its attitude at initial moment and first 5 seconds, and the reference trajectory (red).

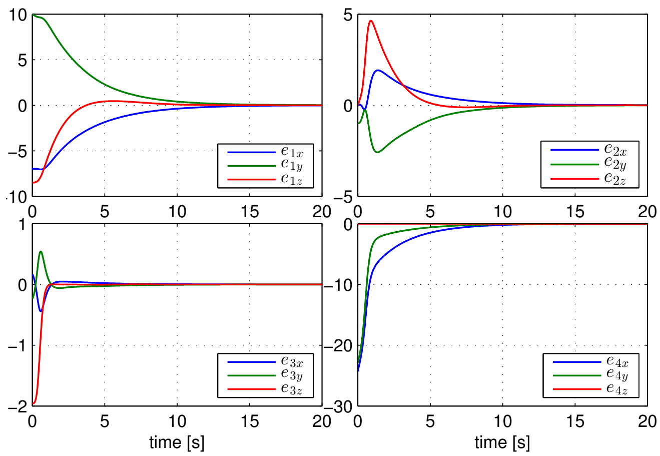

Figure 5. Controller errors over time.

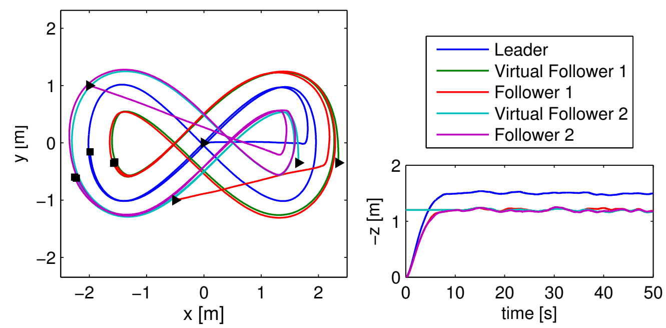

Figure 6. Position of the quadrotors, generated trajectories and reference.

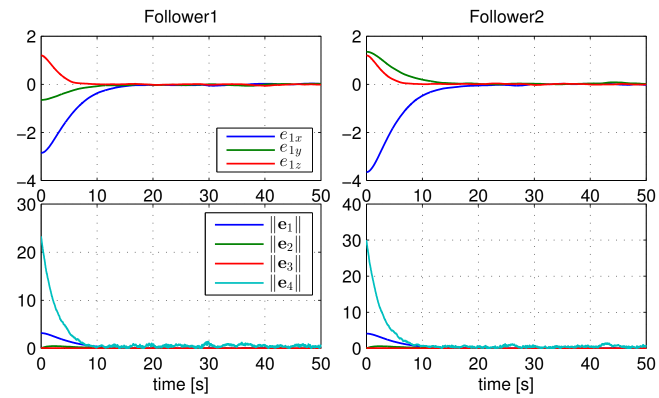

Figure 7. Time evolution of quadrotor's controller errors of both followers.

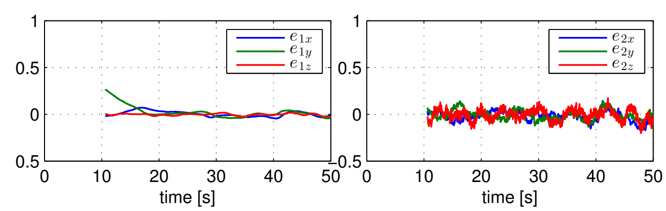

Figure 8. Time evolution of the errors of both virtual followers.

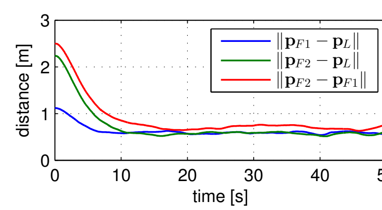

Figure 9. Time evolution of distance between leader and followers (and between them).

As can be seen in figure 5, the time required for the convergence of the errors is approximately 10 seconds. During the first 1 to 2 seconds a faster convergence of the errors $\mathbf{e}_3$ and $\mathbf{e}_4$ is observed, at the cost of growing the error $\mathbf{e}_2$. The first two errors are the slower to converge and even after $t = 10\mathrm{s}$ a reminiscent error is noticeable, vanishing by the end of the simulation.

Quadrotors in formation: The results of a simulation with the trajectory planner and the quadrotor controller are now presented. In this simulation the leader, a quadrotor, is set to follow the same trajectory of the previous simulation. The motion of the leader (position, velocity, and acceleration) is passed to the planner, which generates two different trajectories with identical d_x to be passed as reference to two other quadrotor vehicles.

The quadrotors are initially at rest in the floor. The leader is at $\mathbf{p}_L(0) = [0\ \ 0\ \ 0]^T$, follower 1 at $\mathbf{p}_{F1}(0) = [-0.5\ \ -1\ \ 0]^T$ and follower 2 at $\mathbf{p}_{F2}(0) = [-2\ \ 1\ \ 0]^T$. The vectors $\mathbf{d}$ for each follower were $\mathbf{d}_1 = [0.35\ \ 0.35\ \ -0.3]^T$ and $\mathbf{d}_2 = [0.35\ \ -0.35\ \ -0.3]^T$. The parameters of the controllers of the planner were $k_1 = 0.2$, $k_2 = 2$, $k_3 = 0$, $k_{z1} = 0.2$, $k_{z2} = 2$, and $p_{\max} = 5$.

To assess the robustness of the coordination strategy, noise was added to the state measurement of each quadrotor. As the trajectory generation depend on the leader's state, the addition of noise to the state indirectly introduces noise in the trajectory generation. The noise added is white and gaussian with zero mean and has a standard deviation of $0.2\mathrm{m}$ for the position, $0.1\mathrm{m/s}$ for the linear velocity, $0.01\mathrm{m/s}^2$ for the acceleration, $0.02°/\mathrm{s}$ for the angular velocity and $0.02°$ for the attitude measurement. These values are typical for low cost sensors. In the planar position plot (see figure 3.7), the symbols ▶ represent the initial point of each of the vehicles (both quadrotors and virtual followers) and the symbols ■ their positions at the end of the simulation.

Figure 6 shows that the quadrotors are able to track the trajectories generated by the planner. At the beginning, they rapidly converge to the starting points of the trajectories, while the planner is stopped. Once they approach these points the planner is finally started and the leader starts describing the eight trajectory.

It is noticeable the effect noise has on the trajectory generation. Figure 6 (R) shows that the variations in height of the leader, which were not contained in the reference trajectory, are visible in the height evolution of the followers.

Lastly, figure 9 shows that the distance between quadrotors is kept approximately constant, not varying more than $0.1\mathrm{m}$

between leader and followers and $0.15\mathrm{m}$ between followers, which corresponds to approximately 20% of their average values.

IV. Experimental Evaluation

This section presents the results of an experimental test carried out at the Sensor-Based Cooperative Robotics Research Laboratory – SCORE Lab of the Faculty of Science and Technology of the University of Macau.

Three quadrotors Blade® mQX were employed. These vehicles weigh $78\mathrm{g}$, have a length of $353\mathrm{mm}$ and are actuated in terms of thrust and angular velocity. They are designed to be human piloted with remote controls. However, it was possible to identify the radio chip inside the remote control and connect the serial interface of the RF module to a computer serial port.

A VICON® system, composed of 12 high speed cameras and a set of markers attached to the plants, was used to capture the motion and attitude of the vehicles at $50\mathrm{Hz}$.

Two computers were used in this experiment, one running the VICON software and a Simulink® model which generates the command signals sent to the other computer through Ethernet; and a second one that sends them through serial port to the RF module at $44\mathrm{Hz}$. The decision to separate control and communications was made to avoid jitter in the transmission of the serial-port signals to the RF module. A block diagram of the overall architecture is presented in figure 10.

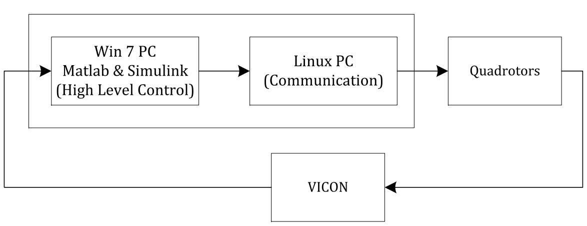

Figure 10. System architecture.

The Simulink model used contains the trajectory planner developed and three quadrotor controllers. This controller is an adaptation of the one presented in [9] and requires the desired position and its derivatives up to the third to be provided. However, in the present test, only position and its first two derivatives were provided.

The VICON system outputs a pre-filtered position of the vehicle and with single differences it is possible to obtain a clean estimation of the velocity. However, double differences are highly contaminated with noise, degrading the performance of the estimation. To overcome this problem it is necessary to low-pass filter the measurements. Using experimental data taken from earlier tests performed with a quadrotor it was possible to test the performance of various filters, with different dimensions. The best trade-off between responsiveness and smoothing was achieved with a moving average filter with 100 coefficients, which introduces a delay of approximately $1\mathrm{s}$.

A. Results

In this experimental test the leader is tracking a trajectory given by

$$\mathbf{p}_{ref} = \begin{bmatrix} \frac{3}{2}\frac{\sin(\gamma/3)}{1+\sin^2(\gamma/3)} \\ \frac{3}{4}\frac{\sin(2\gamma/3)}{1+\sin^2(\gamma/3)} \\ -1.6 \end{bmatrix} \tag{70}$$

where $\dot{\gamma} = \sqrt{1+\sin^2\gamma}$, in order to produce a constant linear speed. The trajectory is rotated by $\pi/4$ counter-clockwise, to better use the space available in the laboratory.

At the beginning of the test the quadrotors are at rest. The leader is at $\mathbf{p}_L(0) = [-1 \ \ 0.48 \ \ 0]^T$, follower 1 at $\mathbf{p}_{F1}(0) = [-0.57 \ \ -0.37 \ \ 0]^T$ and follower 2 at $\mathbf{p}_{F2}(0) = [-1.26 \ \ -0.77 \ \ 0]^T$. The vectors $\mathbf{d}$ for each follower were $\mathbf{d}_1 = [0.35 \ \ 0.35 \ \ -0.3]^T$ and $\mathbf{d}_2 = [0.35 \ \ -0.35 \ \ -0.3]^T$. The parameters of the controllers of the planner were $k_1 = 0.3$, $k_2 = 1.1$, $k_3 = 0.17$, $k_{z1} = 0.2$, $k_{z2} = 1$, and $p_{\max} = 5$.

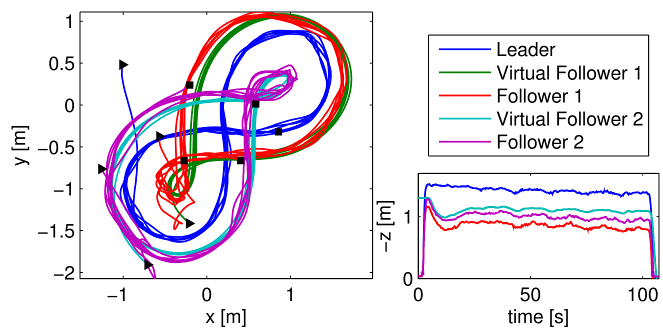

Figure 11. Position of the leader, generated trajectories and followers.

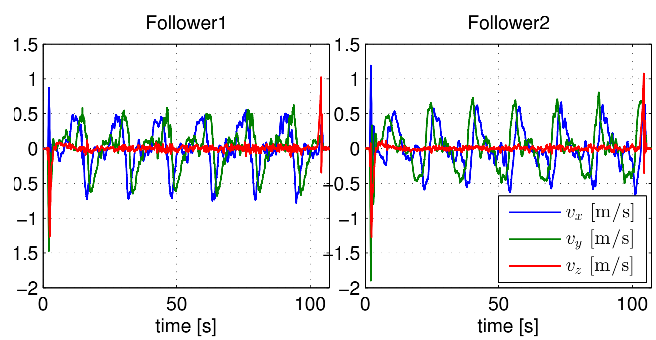

Figure 12. Time evolution of velocities for both the followers.

In figure 14 it is noticeable an oscillatory behaviour of the virtual errors. This oscillation is a result of the gain trade-off found between mitigation of virtual error $\mathbf{e}_1$ and limiting the sensitiveness of the trajectories to the perturbations in leader's movement. It is possible to maintain the virtual errors close to the origin, but at the cost of degrading the performance of the following quadrotors.

The trajectories generated capture the essence of leader's movement, while neglecting the higher frequency perturbations. See for example figure 11 (R), and note the similarities

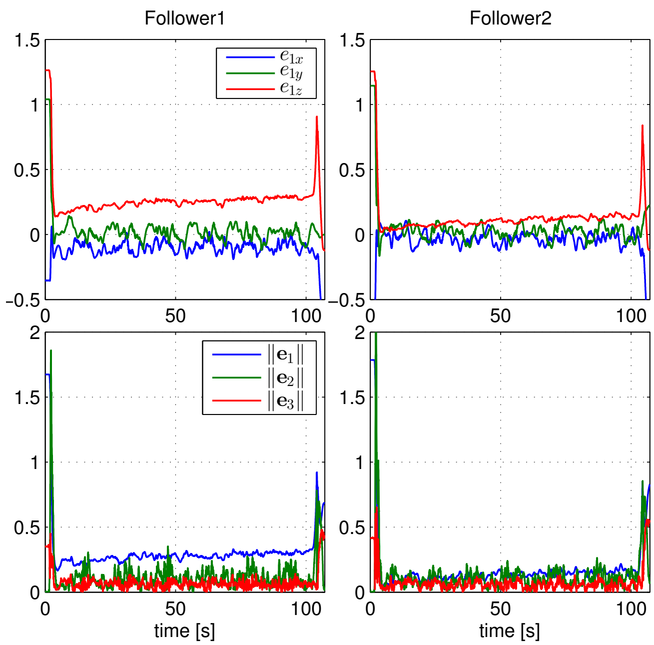

Figure 13. Time evolution of quadrotor's errors for both followers.

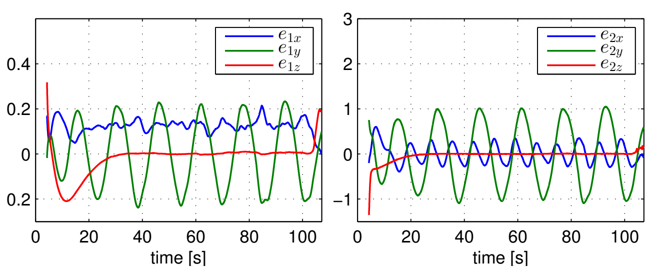

Figure 14. Time evolution of the errors of both virtual followers.

between the dark blue line and the light blue one. The longer and slower variations found in the leader's height can also be found in the height of the virtual followers (the green line cannot be seen for being shadowed by the light blue one). On the other hand, the more instantaneous changes in leader's height are filtered and do not appear in the generated trajectory. This process results in smooth trajectories that can easily be tracked by the controller, as can be seen from the time evolution of velocities and errors (figures 12 and 13).

V. Conclusion

This paper presented a strategy for motion coordination of autonomous vehicles. Concerning the trajectory planner, global and asymptotic convergence of the errors of the virtual vehicles was demonstrated. It has also been shown that when all the virtual followers have equal value of desired longitudinal distance to the leader, the vehicles move in a fixed configuration with respect to a local frame.

The quadrotor controller developed is capable of steering the plant to the desired trajectory, even when started in unfavourable conditions.

Both the simulated and experimental tests of quadrotor formations demonstrated the applicability of the planner to carry out the task, showing that the generated trajectories are easily tracked by aerial vehicles. Although only the leader's position was being measured in the experimental test, the computation of smoothed single and double differences allowed for an accurate tracking of generated trajectories. However, it could be done at the cost of degrading the performance of the planner.

Directions of future work include:

- exploring other possibilities of virtual vehicle models;
- developing collision avoidance capabilities for the planner;
- improving and optimising the motion estimation.

References

[1] P. Ogren, E. Fiorelli, and N. E. Leonard, "Cooperative control of mobile sensor networks: Adaptive gradient climbing in a distributed environment," *IEEE Transactions on Automatic Control*, vol. 49, pp. 1292–1302, 2004.

[2] S. Waharte, N. Trigoni, and S. Julier, "Coordinated search with a swarm of uavs," in *Sensor, Mesh and Ad Hoc Communications and Networks Workshops, 2009. SECON Workshops '09. 6th Annual IEEE Communications Society Conference on*, pp. 1 –3, june 2009.

[3] N. Michael, J. Fink, and V. Kumar, "Cooperative manipulation and transportation with aerial robots," *Autonomous Robots*, vol. 30, pp. 73–86, january 2011.

[4] N. Leonard and E. Fiorelli, "Virtual leaders, artificial potentials and coordinated control of groups," in *Decision and Control, 2001. Proceedings of the 40th IEEE Conference on*, vol. 3, pp. 2968 –2973 vol.3, 2001.

[5] R. Olfati-Saber, "Flocking for multi-agent dynamic systems: algorithms and theory," *Automatic Control, IEEE Transactions on*, vol. 51, pp. 401 – 420, march 2006.

[6] E. Justh and P. Krishnaprasad, "Equilibria and steering laws for planar formations," *Systems and Control Letters*, vol. 52, no. 1, pp. 25 – 38, 2004.

[7] J. Guerrero and R. Lozano, "Flight formation of multiple mini rotorcraft based on nested saturations," in *Intelligent Robots and Systems (IROS), 2010 IEEE/RSJ International Conference on*, pp. 634 –639, October 2010.

[8] P. Kokotovic, "The joy of feedback: nonlinear and adaptive," *Control Systems, IEEE*, vol. 12, pp. 7 –17, june 1992.

[9] D. Cabecinhas, R. Cunha, and C. Silvestre, "Rotorcraft path following control for extended flight envelope coverage," in *Decision and Control, 2009 held jointly with the 2009 28th Chinese Control Conference. CDC/CCC 2009. Proceedings of the 48th IEEE Conference on*, pp. 3460 –3465, dec. 2009.